# Authors' Response to Reviews of

Secondary Ice Formation in Cumulus Congestus Clouds: Insights from Observations and Aerosol-Aware Large-Eddy Simulations

Silvia M. Calderón, Noora Hyttinen, Harri Kokkola,Tomi Raatikainen, R. Paul Lawson, and Sami Romakkaniemi
*Atmospheric Chemistry and Physics,* https://doi.org/10.5194/egusphere-2025-2730

---

**RC: *Reviewers' Comment***, AR: Authors' Response, ☐ Manuscript Text

## Reviewer #2

https://doi.org/10.5194/egusphere-2025-2730-RC2

## 1. Overall comments

**RC:** The manuscript is undoubtedly a work of very high degree of complexity, so it was a challenge for me (not a modeler) to follow the discussion of various processes and feedback mechanisms associated with secondary ice formation. Nevertheless, I feel that this is exactly the type of modelling study needed to bridge the gaps between the patchy snapshots obtained via airborne in-situ observations, lab studies conducted under poorly-defined conditions, and simplified cloud modelling where parameterizations of SIP rates are based on incomplete lab data and wild extrapolations. I therefore recommend publication of the manuscript after several minor issues have been addressed.

AR: We deeply appreciate your insightful analysis, comments and suggestions. We will proceed to address your indications one by one.

## 2. Detailed comments

### 2.1.

**RC:** I have a general comment on the choice of parameterization of h(T) for DS mechanism: since (Leisner 2014) there was a number of experimental studies of DS mechanism Keinert et al. [2020], Kleinheins et al. [2021], Lauber et al. [2018] that, even if not covering the whole parameter space, have specifically addressed more realistic freezing conditions. These studies have demonstrated, that in comparison to parameterizations based on (Lawson et al., 2015) and later used by (Sullivan et al., 2018), the number of secondary ice particles produced by a single freezing droplet should be enhanced for free fall conditions (Keinert et al., 2020) and could be even higher by factor 4 to 7 if considering the pressure release events as indicators for secondary ice production (Kleinheins et al., 2021). So maybe the parameterization used here is not the greatest choice.

AR: You are right, there are recent studies that have addressed more realistic freezing conditions. We were aware of them, but decided to keep the parameterizations in their original form to compare our results with other cloud modelling studies. Also, we did not know up to what point the results from single-droplet size experiments could be translated into the whole parameter space. Nonetheless, we have compiled their results in Figure 1 that shows temperature dependence of the frequency of droplet shattering events for pure water

droplets levitated in an electrodynamic balance Lauber et al. [2018] and also exposed to a counter-current flow of moist air to reproduce their fall at terminal velocity Keinert et al. [2020], Kleinheins et al. [2021]. For comparison purposes, we have also included the the variation of the ratio $\frac{IMF}{IMF_{max}}$ along the temperature range given by the parametrization of Phillips et al. [2018]. This ratio implicitly isolates the hydrometeor size effects from the temperature dependence of the ice multiplication factor (IMF) reflecting the modeled frequency of droplet shattering events for pure water droplets. The shape in the variation trend of the ratio $\frac{IMF}{IMF_{max}}$ also reflects the $h\left(T\right)$ function included in Equation 16 by Phillips et al. [2018] to account for temperature effects in their simplified or semi-theoretical formulation of the mode 1. The mode 1 describes the possibility of droplet fragmentation during freezing when ice expansion produces an internal pressure strong enough to crack the ice shell leading to the formation of secondary ice particles. Although in its original formulation, this parameterization estimates large and tiny secondary ice fragments, in our study we did not implement this distinction. Kleinheins et al. [2021] reports higher probability of SIP-DS occurrence across the temperature range with values that decrease with increasing temperature unlike other experimental studies. The frequency of occurrence of SIP-DS in the experiments of Lauber et al. [2018] and Keinert et al. [2020] reaches maximum probabilities between -15°C and -10°C in consonance with the temperature-dependence of the parameterization of Phillips et al. [2018]. However, the discrepancies observed between the model and experimental studies, and even among experiments themselves, emphasize the importance of conducting further experiments to reassess existing parameterizations.

**2.2.**

**RC:** Lines 163-166: "In this study, we keep the conventional assumption that the rime splintering mechanism generates single-size ice crystals in the shape of hexagonal columns with a density of 917 $\mathrm{gm}^{-3}$ and a maximum length of 10 $\mu$m ... Bühl et al. [2019].

**RC:** (Bühl et al., 2019) does not discuss the size and shape of ice splinters produced in rime-splintering mechanism. I am also not aware of any other study citing "conventional assumption" that such crystals are generated in an RS SIP. In fact, from the mechanistic point of view this is not very plausible assumption, since RS is supposed to produce secondary ice upon riming of ice by droplets that are themselves in the size range between 10 $\mu$m and 30 $\mu$m. This would require splintering of the whole frozen droplets or quite large fragments of the frozen droplets upon collision with ice. Neither that nor freezing of a supercooled droplets upon glancing contact with the ice, another mechanism that would produce secondary ice in this size range, has not been observed in the recent experimental study of Seidel et al. [2024].

AR: You are right. Our statement requires rephrasing to reflect properly our assumptions. We used the mass-diameter relationship for hexagonal columns reported by Bühl et al. [2019] to calculate the splinter mass. We modified the manuscript text to clarify this point. In the simpler approaches, splinter formation is modeled as a mass transfer from the snow class to the cloud ice by assuming assuming ice crystals of constant size, for example, 10 $\mu$m in diameter Morrison et al. [2005] or ice particles of 20 $\mu$m in diameter and $3.76\times10^{-12}$ kg [Ziegler et al., 1986]. Other assume that splinters have a fixed mass equal to $1\times10^{-12}$ kg [Reisner et al., 1998], or $2.09\times10^{-15}$ kg [Zhao et al., 2021]. Other impose a crystal habit assuming splinters as columnar crystals of maximum length of 12 $\mu$m Mansell et al. [2010] or columnar ice crystals of 30 $\mu$m with mass of $8.5710\times10^{-12}$ kg Mansell and Ziegler [2013]. More complex approaches assume that the splinter mass depends on the parent drop mass with a maximum mass of $1.71\times10^{-11}$ kg Grzegorczyk et al. [2025]. Our assumption goes in consonance with these approaches, as we assumed that splinters are hexagonal columns with length of 10 $\mu$m that correspond to a mass of $3.1227\times10^{-13}$ kg.

AR: Your statement about the splinter/drop relative size is valid from the microscopical point of view. In our study, we simulated splinter formation as the result of collisions between populations of droplets (i.e. diameter above

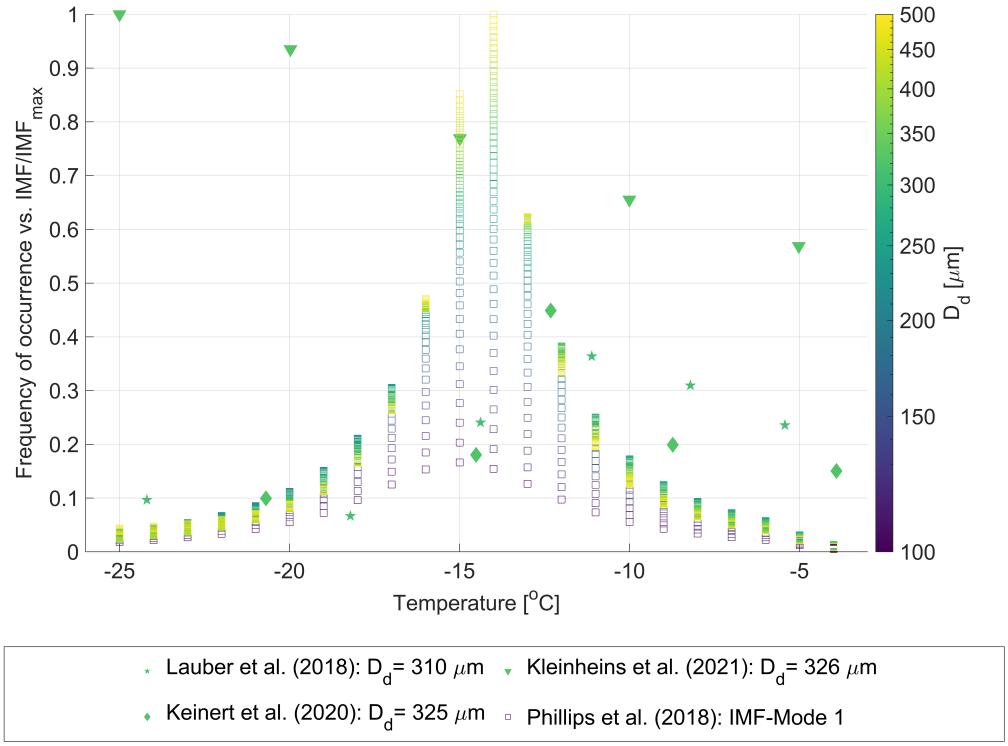


Figure 1: Frequency of occurrence of secondary ice production by droplet shattering (SIP-DS) in experiments with pure water droplets compared to the temperature dependence of the ice multiplication factor (IMF) in the SIP-DS parametrization of Phillips et al. [2018] expressed through the ratio $\frac{IMF}{IMF_{max}}$. Mode 1 and Mode 2 refer to the collision type leading to secondary ice production, $D_d > D_i$ and $D_d < D_i$, respectively.

24 $\mu$m) with larger ice crystals. The number of splinters produced depends on the collected liquid mass corresponding to a number of droplet-ice collisions and follows the Hallet–Mossop factor of 350 splinters per milligram of rimed ice Hallet and Mossop [1974]. If there were $2\times10^9$ droplet-ice collisions involving the riming of a monodisperse droplet population of 24 $\mu$ m-diameter, only 5 splinters would be produced.

> In this study, we assumed~~keep the conventional assumption~~that the rime splintering mechanism generates single-size ice crystals in the shape of hexagonal columns with a mass equal to $3.1227\times10^{-13}$ kg~~with a density of 917 gm$^{-3}$~~and a maximum length of 10 $\mu$m . We used the mass-diameter relationship reported by Buhl et al.(2019) for hexagonal columns to calculate the mass of a splinter.~~(i.e. mi = 110.7983$D^2$.91 (Bühl et al., 2019)).~~

**2.3.**

**RC:** Line 164: The density of "917 gm$^{-3}$ " doesn't make any sense. It should be kg x m$^{-3}$ or 0.917 g x cm$^{-3}$.

AR: Thank you for pointing out this mistake. We eliminated the typo.

**2.4.**

**RC:** Lines 165-166: "Instead, we assume that the mechanisms of droplet shattering and ice–ice collisional breakup generate ice crystals that can range in size from 2 $\mu$m to nearly as large as the fragmenting hydrometeor (i.e. supercooled droplet or ice crystal)." Why "instead"? This sentence relates to a different mechanism, doesn't it?

AR: Yes, you are right. It was a bad choice of words.

> ~~Instead, w~~We assumed that the mechanisms of droplet shattering and ice–ice collisional breakup generate ice crystals that can range in size from 2 $\mu$m to nearly as large as the fragmenting hydrometeor (i.e. supercooled droplet or ice crystal).

**2.5.**

**RC:** Lines 167-169: "We distribute the total number of secondary ice particles NSIP (T,Dl,Dm) produced by a collision between two hydrometeors of size Dl and Dm between size bins smaller than the fragmenting hydrometeor in such a way that each bin gains the same amount of mass, similar to Lawson et al. (2015)." Lawson et al., (2015) distributes the number of crystals evenly across all the bins, not the mass: The secondary ice produced is distributed evenly over a range of ice size bins that are smaller than the diameter of the original frozen drop (their page 2442). Also, (Lawson et al., 2015) considers exclusively droplet shattering (DS) as the sole SIP mechanism in their study, the RS and the IIBR are not discussed.

AR: You are right. It was a misunderstanding from our part. We have corrected the text in the manuscript as follows:

> We distribute the total number of secondary ice particles $N_{\mathrm{SIP}}\,(T, D_l, D_m)$ produced by a collision between two hydrometeors of size $D_l$ and $D_m$ between size bins smaller than the fragmenting hydrometeor in such a way that each bin gains the same amount of mass ~~, similar to Lawson et al. (2015)~~. This means that secondary ice particle size distribution follows a $D^{-3}$-powerlaw distribution with a minimum fragment size D of 2$\mu$m. This relationship aligns with the model of fractal crushing used to describe

the scale-invariant low energy fragmentation of brittle materials (Palmer and Sanderson, 1991; Weiss, 2001; Åström et al., 2021).

**2.6.**

**RC:** Section 2.2, Table 1 and discussion thereof: It is difficult to follow the comparison between various descriptions of size and number distribution of secondary ice particles. Why don't you give the functional form of these distributions for all three SIP mechanisms as functions of hydrometeors' size, ambient parameters, and factors affecting collision events?

AR: Great suggestion. We added Tables 1 and 2 with the functional forms for the ice multiplication factor IMF used in parameterizations of secondary ice production rates through the mechanisms of rime splintering (SIP-RS) and droplet shattering (SIP-DS), and ice-ice collisional breakup (SIP-IIBR). We have added the limiting sizes affecting collision events as well as the maximum size of secondary ice particles produced per SIP event in each mechanism. A list of symbols summarizes the description of the most relevant variables. We added indications about the factors affecting collision kernels via settling velocities Beard [1976], Khvorostyanov and Curry [2002] Morrison and Milbrandt [2015]. Due to their large size, we moved them to the supporting information. The text in the manuscript was modified as follows:

Parametrizations for IMF and triggering conditions reported in literature vary widely for a single mechanism. Because these differences affect SIP rates, we have set up a common set of modeling constraints reported in ~~Table S1 together with the limiting size used for the mass distribution of secondary ice particles.~~in Table S1 and Table S2 together with the limiting size used for the mass distribution of secondary ice particles. After a secondary ice production event, secondary ice particles follow a number size distribution of the power-law type $D^{-3}$ with $D$ representing the hydrometeor size (i.e. diameter or maximum length). Secondary ice particles are located in ice bins smaller than the hydrometeor that generates them. In all cases, collision kernels are calculated using settling velocities that depend on air properties and diameter in the case of droplets (Beard, 1976), and also on the crystal habit whose mass-diameter and area-diameter relationships vary according to the rime fraction in the case of ice particles (Khvorostyanov and Curry,2002; Morrison and Milbrandt, 2015.

**2.7.**

**RC:** Figure 5 seems to have no legend, which makes it impossible to follow the discussion.

AR: Please receive our apologies. It was an unfortunate mistake. We have included here Figure 5 for the sake of completeness.

**2.8.**

**RC:** Figure 6: I don't see three "...Continuous black lines indicate altitudes at which temperatures are 273.15 K, 265.15 K and 258.15 K". There are only two black lines per panel, I assume the coldest one is missing?

AR: At 40 min, the cloud has not reached 258.15 K and therefore the temperature contour plot does not draw an isotherm at that level. Later in the simulation, the three isotherms for 273.15 K, 265.15 K and 258.15 K appeared clearly in the mixed-phase zone as shown in Figures 7 and 8. We modified the figure caption as follows:

Table 1: Functional forms for the ice multiplication factor IMF in parameterizations of secondary ice production rates through the mechanisms of rime splintering (SIP-RS) and droplet shattering (SIP-DS). Variables $D_d, D_i, D_{sip}$ refer to the size of droplets in m if there are no additional indications (i.e. cloud droplet or precipitation droplet), ice particles, and secondary ice particles, respectively. $m_d, m_i$ refer to the droplet mass and the ice particle mass in kg. $v_d, v_i$ refer to the settling velocity of the droplet and the ice particle in m s$^{-1}$, respectively. $\rho_w$ refers to the water density in kg m$^{-3}$, $c_w$ refers to the specific heat capacity of liquid water in J K$^{-1}$kg$^{-1}$. $L_f$ refers to the specific latent heat of freezing in K kg$^{-1}$, while $\gamma_{liq}$ is the surface tension of liquid water in J m$^{-2}$. $T$ is the drop freezing temperature in °C that in our model is assumed to be the moist air temperature.

SIP-RS*: mostly active at temperatures from -8°C to -2°C [Hallet and Mossop, 1974]

A droplet-ice collision leads to secondary ice production if $(D_d > 24\mu m \wedge D_d < D_i)$

$D_{sip} = 10\mu m$

$$\text{IMF} = 3.5 \times 10^8 E(T) \frac{\pi}{6} D_d^3 \rho_w$$

$$E(-2 < T < 0) = 0.05,\ E(-2 \leq T < -4) = 0.5$$

$$E(-4 \leq T < -6) = 1,\ E(-6 \leq T \leq -8) = 0.5$$

$$E(T < -8) = 0.05$$

*In this study we have assumed a 5% efficiency of SIP-RS at subzero temperatures outside this range.

SIP-DS-Mode 1: active at temperatures from -28°C to -3°C [Phillips et al., 2018]

A droplet-ice collision leads to secondary ice production if $(D_d > 50\mu m \wedge D_d > D_i)$

$D_{sip} < D_d$

$$\text{IMF} = \min\left(\left(\frac{\zeta \eta^2}{(T - T_o) + \eta^2} + \beta T\right), 100\right)$$

$$X = \log_{10}(D\,[mm])$$

$$\beta(D_d < 400\mu m) = 0 \quad T_o(D_d < 50\mu m) = 0$$

$$\log_{10}\zeta(D_d < 50\mu m) = 0 \quad \log_{10}\eta(D_d < 50\mu m) = 0$$

$$\beta(50\mu m \leq D_d \leq 1600\mu m) = \left(-0.1839X^2 - 0.2017X - 0.0512\right)$$

$$\log_{10}\zeta(50\mu m \leq D_d \leq 1600\mu m) = \left(2.4268X^3 + 3.3274X^2 + 2.0783X + 1.2927\right)$$

$$\log_{10}\eta(50\mu m \leq D_d \leq 1600\mu m) = \left(0.1242X^3 - 0.2316X^2 - 0.9874X - 0.0827\right)$$

$$T_o(50\mu m \leq D_d \leq 1600\mu m) = \left(-1.3999X^3 - 5.3285X^2 - 3.9847X - 15.0332\right)$$

When $D_d > 1600$ $\mu$m, the value of $D_d$ used for the polynomials was 1600 $\mu m$ without linear extrapolation of IMF as in the original formulation.

SIP-DS- Mode 2: active at temperatures from -28°C to -3°C [Phillips et al., 2018]

A droplet-ice collision leads to secondary ice production if $(D_d > 50\mu m \wedge D_i > D_d)$

$D_{sip} < D_d$

$$\text{IMF} = \min\left(\Phi(T)(1 - f(T)) \max\left(\frac{K_0}{\gamma_{\text{liq}} \pi D_d^2} - 0.2, 0\right), 100\right)$$

$$K_0 = 0.5 \frac{m_d m_i}{m_d + m_i} (v_d - v_i)^2$$

$$f(T) = -\frac{c_w T}{L_f}$$

$$\Phi(T) = min(1, 4f(T))$$

Table 2: Functional forms for the ice multiplication factor IMF in the parameterization of secondary ice production rates through the mechanisms of ice–ice collisional breakup (SIP-IIBR). Variables $D_i, D_{sip}$ refer to the size of ice particles, and secondary ice particles, respectively in m. $D_{i1}$ refers to the smallest ice particle that breaks with a equivalent spherical surface area equal to $\alpha$ in m$^{-2}$. $T$ is the temperature in K. $K_0$ refers to the collision kinetic energy in J. $S_i$ refers to the water supersaturation over ice. $A_M$ refers to the number density of breakable asperities in region of contact, and $a_o$ is the maximum $A_m$, both in m$^{-2}$. $C$ refers to the asperity-fragility coefficient in J, and $\phi$ is the fraction of rimed ice.

| SIP-IIBR: active at temperatures from -28°C to -3°C [Phillips et al., 2018]-[Grzegorczyk et al., 2025] | |
|---|---|
| An ice-ice collision leads to secondary ice production if $(D_{i,1} > 4\mu m \wedge D_{i,2} > D_{i,1})$ | |
| Ice-ice collisions are affected by the aggregation efficiency $E_{\text{agg}}(\phi) = 0.30 - 0.25\phi$ | |
| $D_{sip} < D_{i1}$ | $\text{IMF} = \min\left(\alpha A_M \left(1 - \exp\left(-\left(\frac{CK_0}{\alpha A_M}\right)^{\gamma}\right)\right), 600\right)$ |
| | $A_M = \frac{a_o}{3} + \max\left(\frac{2a_o}{3} - \frac{a_o}{9}\lvert T - 258.15\rvert, 0\right)$ |
| | $\alpha = \pi D_{i1}^2$ |
| [Sotiropoulou et al., 2021] [Mizuno, 1990] | $K_0 = \frac{m_{i1}m_{i2}}{m_{i1}+m_{i2}}\left(1.7\left(v_{i1}-v_{i2}\right)^2 + 0.3 v_{i1} v_{i2}\right)$ |
| Unrimed particle $(\phi < 0.5)$ | $a_0 = 4.75 \times 10^7$ |
| | $C = 1 \times 10^8$ |
| | $\gamma = 0.78$ |
| Rimed particle $(\phi >= 0.5)$ | $a_0 = \exp(14.74 S_i + 14.28)$ |
| (P. Grzegorczyk, personal communication, | $C = \exp(20.15 S_i + 13.78)$ |
| January 03, 2025) | $\gamma = S_i + 0.55$ |

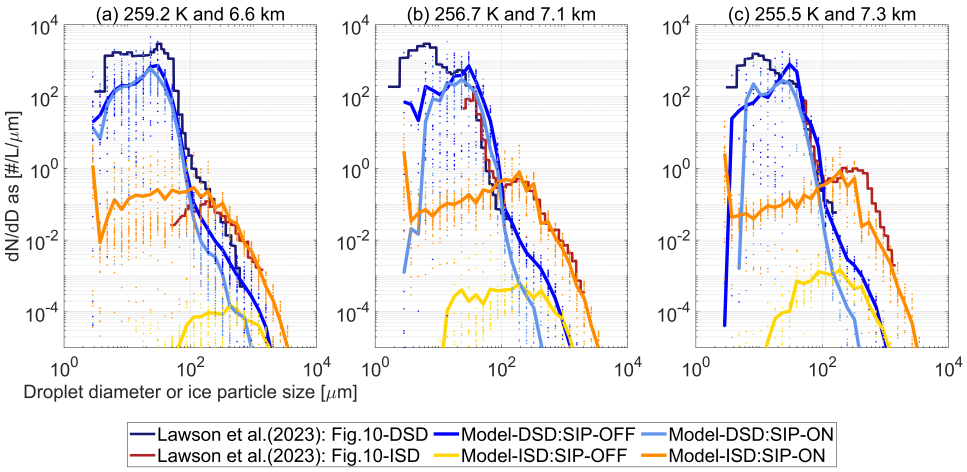


Figure 2: Ice particle size distributions in updrafts at altitudes of (a) 2.6 km above freezing level (b) 3.2 km above freezing level (c) 400 m below cloud top. Observations were taken from Figure 10 in Lawson et al. [2023]. Modeled values are shown as mean horizontal values with dotted lines along size bins indicating variability across cloudy points with mixed-phase conditions defined as LWC $>$ 0.01 gm$^{-3}$, IWC $>$ 0.001 gm$^{-3}$ and updraft velocity $>$ 0.02 m s$^{-1}$.

Vertical profile of liquid water content (LWC) and ice water content (IWC) at 40 min after convection initiation. Contour lines in gray indicate Total Water Content (TWC) values of 0.01 gm$^{-3}$ and 3.5 gm$^{-3}$ to enclose cloudy and core conditions. Continuous black lines indicate altitudes at which temperatures are 273.15 K, and265.15 K ~~and 258.15 K~~corresponding to freezing, andmaximum ice multiplication by rime splintering ~~and by droplet shattering~~, respectively. Panels (a-b) Simulation scenario without secondary ice processes. Panel (c-d) Simulation scenario with secondary ice processes.

**2.9.**

**RC:** Figure 7: why are the SIP-RS rates in the temperature range below -10°C (above the black line corresponding to 263.15 K in the panes d) and g) of the figure 7) non-zero? Should it not be strictly allocated to the temperature range between -3°C and -8°C (as indicated by parameterization in the table 1)? Same questions regarding Figure 11, panel a).

AR: Good point. We assumed an efficiency of 5% for all values outside this temperature range as indicated in the first footnote of Table 1.

**2.10.**

**RC:** The difference in color in the color-coded lines in the Figure 12 panels a) and b) is hardly visible. Maybe use a different color palette?

AR: Thank you. It is a very good suggestion. A new version of Figure 12 have been added to the manuscript, and it is included here for the sake of completeness.

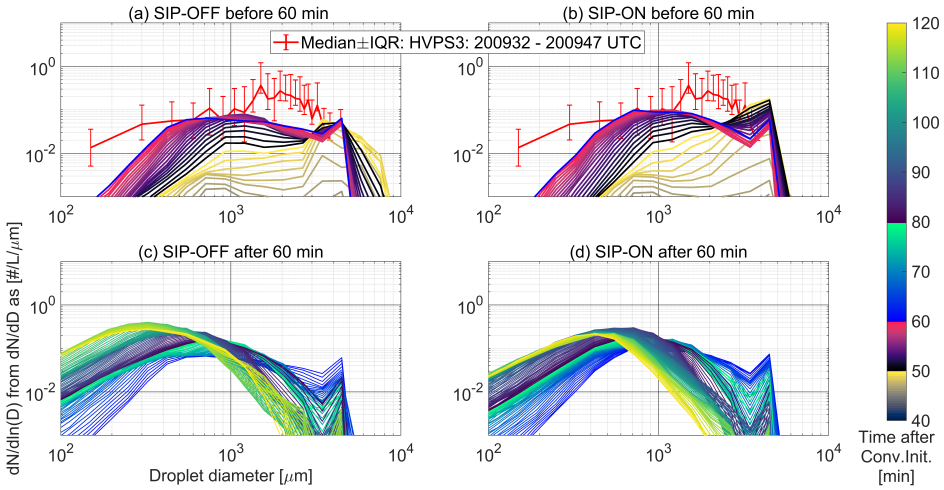


Figure 3: Temporal variation of droplet size distributions below cloud base at an altitude of 1.05 km compared to droplet size distributions derived from the High Volume Precipitation Spectrometer (HVPS3) measured at 1.03 km. Modeled outputs were represented using average size distributions in cloudy points. Distributions are color coded to follow the simulation time after convection initiation. Panel (a) SIP-OFF scenario in the first simulation hour. Panel (b) SIP-ON scenario in the first simulation hour. Panel c) SIP-OFF scenario in the second simulation hour. Panel (d) SIP-ON scenario in the second simulation hour.

## References


K. V. Beard. Terminal velocity and shape of cloud and precipitation drops aloft. *Journal of Atmospheric Sciences*, 33(5):851 – 864, 1976. . URL https://journals.ametsoc.org/view/journals/atsc/33/5/1520-0469_1976_033_0851_tvasoc_2_0_co_2.xml.

J. Bühl, P. Seifert, M. Radenz, H. Baars, and A. Ansmann. Ice crystal number concentration from lidar, cloud radar and radar wind profiler measurements. *Atmospheric Measurement Techniques*, 12:6601–6617, 2019. . URL https://amt.copernicus.org/articles/12/6601/2019/.

P. Grzegorczyk, W. Wobrock, A. Canzi, L. Niquet, F. Tridon, and C. Planche. Investigating secondary ice production in a deep convective cloud with a 3d bin microphysics model: Part i - sensitivity study of microphysical processes representations. *Atmospheric Research*, 313:107774, 2025. ISSN 0169-8095. . URL https://www.sciencedirect.com/science/article/pii/S0169809524005568.

J. Hallet and S. C. Mossop. Production of secondary ice particles during the riming process. *Nature*, 249: 26–28, 1974. ISSN 1476-4687. .

A. Keinert, D. Spannagel, T. Leisner, and A. Kiselev. Secondary ice production upon freezing of freely falling drizzle droplets. *Journal of the Atmospheric Sciences*, 77:2959 – 2967, 2020. . URL https://journals.ametsoc.org/view/journals/atsc/77/8/jasD200081.xml.

V. I. Khvorostyanov and J. A. Curry. Terminal velocities of droplets and crystals: Power laws with continuous parameters over the size spectrum. *Journal of the Atmospheric Sciences*, 59(11):1872 – 1884, 2002.

. URL https://journals.ametsoc.org/view/journals/atsc/59/11/1520-0469_2002_059_1872_tvodac_2.0.co_2.xml.

J. Kleinheins, A. Kiselev, A. Keinert, M. Kind, and T. Leisner. Thermal imaging of freezing drizzle droplets: Pressure release events as a source of secondary ice particles. *Journal of the Atmospheric Sciences*, 78(5): 1703 – 1713, 2021. . URL https://journals.ametsoc.org/view/journals/atsc/78/5/JAS-D-20-0323.1.xml.

A. Lauber, A. Kiselev, T. Pander, P. Handmann, and T. Leisner. Secondary ice formation during freezing of levitated droplets. *Journal of the Atmospheric Sciences*, 75(8):2815 – 2826, 2018. . URL https://journals.ametsoc.org/view/journals/atsc/75/8/jas-d-18-0052.1.xml.

R. P. Lawson, A. V. Korolev, P. J. DeMott, A. J. Heymsfield, R. T. Bruintjes, C. A. Wolff, S. Woods, R. J. Patnaude, J. B. Jensen, K. A. Moore, I. Heckman, E. Rosky, J. Haggerty, R. J. Perkins, T. Fisher, and T. C. J. Hill. The secondary production of ice in cumulus experiment (spicule). *Bulletin of the American Meteorological Society*, 104:E51 – E76, 2023. . URL https://journals.ametsoc.org/view/journals/bams/104/1/BAMS-D-21-0209.1.xml.

E. R. Mansell and C. L. Ziegler. Aerosol effects on simulated storm electrification and precipitation in a two-moment bulk microphysics model. *Journal of the Atmospheric Sciences*, 70(7):2032 – 2050, 2013. . URL https://journals.ametsoc.org/view/journals/atsc/70/7/jas-d-12-0264.1.xml.

E. R. Mansell, C. L. Ziegler, and E. C. Bruning. Simulated electrification of a small thunderstorm with two-moment bulk microphysics. *Journal of the Atmospheric Sciences*, 67(1):171 – 194, 2010. . URL https://journals.ametsoc.org/view/journals/atsc/67/1/2009jas2965.1.xml.

H. Mizuno. Parameterization of the accretion process between different precipitation elements. *Journal of the Meteorological Society of Japan*, 68(3):395–398, 1990. .

H. Morrison and J. A. Milbrandt. Parameterization of ice microphysics based on the prediction of bulk particle properties. part i: Scheme description and idealized tests. *J. Atmos. Sci.*, 72:287–311, 2015.

H. Morrison, J. A. Curry, and V. I. Khvorostyanov. A new double-moment microphysics parameterization for application in cloud and climate models. part i: Description. *Journal of the Atmospheric Sciences*, 62: 1665 – 1677, 2005. . URL https://journals.ametsoc.org/view/journals/atsc/62/6/jas3446.1.xml.

V. T. J. Phillips, S. Patade, J. Gutierrez, and A. Bansemer. Secondary ice production by fragmentation of freezing drops: Formulation and theory. *Journal of the Atmospheric Sciences*, 75:3031–3070, 2018. . URL https://journals.ametsoc.org/view/journals/atsc/75/9/jas-d-17-0190.1.xml.

J. Reisner, R. M. Rasmussen, and R. T. Bruintjes. Explicit forecasting of supercooled liquid water in winter storms using the mm5 mesoscale model. *Quarterly Journal of the Royal Meteorological Society*, 124 (548):1071–1107, 1998. . URL https://rmets.onlinelibrary.wiley.com/doi/abs/10.1002/qj.49712454804.

J. S. Seidel, A. A. Kiselev, A. Keinert, F. Stratmann, T. Leisner, and S. Hartmann. Secondary ice production – no evidence of efficient rime-splintering mechanism. *Atmospheric Chemistry and Physics*, 24(9):5247–5263, 2024. . URL https://acp.copernicus.org/articles/24/5247/2024/.

G. Sotiropoulou, E. Vignon, G. Young, H. Morrison, S. J. O'Shea, T. Lachlan-Cope, A. Berne, and A. Nenes. Secondary ice production in summer clouds over the antarctic coast: an underappreciated process in atmospheric models. *Atmospheric Chemistry and Physics*, 21(2):755–771, 2021. . URL https://acp.copernicus.org/articles/21/755/2021/.

X. Zhao, X. Liu, V. T. J. Phillips, and S. Patade. Impacts of secondary ice production on arctic mixed-phase clouds based on arm observations and cam6 single-column model simulations. *Atmospheric Chemistry and Physics*, 21(7):5685–5703, 2021. . URL https://acp.copernicus.org/articles/21/5685/2021/.

C. L. Ziegler, P. S. Ray, and D. R. MacGorman. Relations of kinematics, microphysics and electrification in an isolated mountain thunderstorm. *Journal of Atmospheric Sciences*, 43(19):2098 – 2115, 1986. . URL https://journals.ametsoc.org/view/journals/atsc/43/19/1520-0469_1986_043_2098_rokmae_2_0_co_2.xml.